ornl

OAK RIDGE NATIONAL LABORATORY

MARTIN MARIETTA

ORNL/TM-11816

MARTIN MARIETTA ENERGY SYSTEMS LIBRARIES

3 4456 0324639 7

Heat Transfer Effectiveness of a Thermal Barrier Coating With Different Fuel Compositions

N. Domingo

OAK RIDGE NATIONAL LABORATORY
CENTRAL RESEARCH LIBRARY
CIRCULATION SECTION
4500N ROOM 175
LIBRARY LOAN COPY
DO NOT TRANSFER TO ANOTHER PERSON
If you wish someone else to see this report, send in name with report and the library will arrange a loan.

MANAGED BY
MARTIN MARIETTA ENERGY SYSTEMS, INC.
FOR THE UNITED STATES
DEPARTMENT OF ENERGY

This report has been reproduced directly from the best available copy.

Available to DOE and DOE contractors from the Office of Scientific and Technical Information, P.O. Box 62, Oak Ridge, TN 37831; prices available from (615) 576-8401, FTS 626-8401.

Available to the public from the National Technical Information Service, U.S. Department of Commerce, 5285 Port Royal Rd., Springfield, VA 22161.

This report was prepared as an account of work sponsored by an agency of the United States Government. Neither the United States Government nor any agency thereof, nor any of their employees, makes any warranty, express or implied, or assumes any legal liability or responsibility for the accuracy, completeness, or usefulness of any information, apparatus, product, or process disclosed, or represents that its use would not infringe privately owned rights. Reference herein to any specific commercial product, process, or service by trade name, trademark, manufacturer, or otherwise, does not necessarily constitute or imply its endorsement, recommendation, or favoring by the United States Government or any agency thereof. The views and opinions of authors expressed herein do not necessarily state or reflect those of the United States Government or any agency thereof.

ORNL/TM-11816

Engineering Technology Division

HEAT TRANSFER EFFECTIVENESS OF A THERMAL BARRIER COATING WITH DIFFERENT FUEL COMPOSITIONS

N. Domingo

June 1991

NOTICE This document contains information of a preliminary nature. It is subject to revision or correction and therefore does not represent a final report.

Prepared by the
Oak Ridge National Laboratory
Oak Ridge, Tennessee 37831
managed by
MARTIN MARIETTA ENERGY SYSTEMS, INC.
for the
U.S. DEPARTMENT OF ENERGY
under contract DE-AC05-840R21400

MARTIN MARIETTA ENERGY SYSYEMS LIBRARIES

3 4456 0324639 7

CONTENTS

	Page
ABSTRACT	1
1. INTRODUCTION	1
2. DESCRIPTION OF TEST APPARATUS	4
2.1 BURNER	4
2.2 TEST SECTION	4
2.3 STEAM GENERATOR	8
3. TEST SPECIMEN	9
4. OPERATING PROCEDURE AND INSTRUMENTATION	12
4.1 STEADY-STATE OPERATION	12
4.2 INSTRUMENTATION AND DATA ACQUISITION	14
4.3 LASER-FLUORESCENCE THERMOMETRY	14
5. CHARACTERISTICS OF GRAY CAST IRON AND THERMAL BARRIER COATING IN TEST SPECIMEN	18
6. TEST PLAN	22
7. HEAT TRANSFER ANALYSIS	23
8. RESULTS AND DISCUSSION	26
9. CONCLUSIONS	32
10. FUTURE WORK	33
ACKNOWLEDGEMENTS	34
REFERENCES	35

HEAT TRANSFER EFFECTIVENESS OF A THERMAL BARRIER COATING WITH DIFFERENT FUEL COMPOSITIONS

N. Domingo

ABSTRACT

Experiments were conducted to determine the heat transfer effectiveness of a plasma-sprayed, partially stabilized, zirconia coating when heated by a non-luminous, less radiant flame (methane/air) and a luminous flame (n-butane/air). Composite thermal conductances (combined conductive and radiative resistance) are reported for a 0.5-mm thick ceramic coating at a given heat flux and coating mean temperature. A novel laser-fluorescence thermometry technique, which has been shown to be independent of flame thermal radiation background and surface emissivity, was used to measure coating surface temperature. Without reheating, the results showed that the thermal conductance decreased by 66% with temperature within the range of 170°-240°C. For n-butane flame heating, the thermal conductance decreased by 54% over a very narrow temperature range. Reheating of the coating produced an apparent irreversible change in its thermal conductance. Initial values for thermal conductance decreased by 30% following reheat.

1. INTRODUCTION

The choice of a thermal barrier material that is optimum for an alternative-fueled diesel engine and a diesel-fueled low heat rejection engine (LHR) is not a simple or clear task. A recent ORNL assessment [1] of LHR engine research work identified inconsistencies and contradictions between experimental and predicted performance results. Almost all

computer simulation studies on LHR engines predict improved thermal efficiency, reduced heat rejection to coolant, and increased exhaust availability relative to conventionally cooled ones. On the other hand, experimental results have cast serious doubts on the validity of predictions: some have been inconclusive, the majority have contradicted predicted results. Several plausible explanations have been suggested to explain the controversy. One problem is that differences in heat transfer analysis (global versus local) are employed to obtain comparative results. Also, not all loss terms are accounted for in modelling the combustion characteristics of a LHR combustion chamber. One particular loss issue is the degradation of heat transfer in thermal barrier coatings over time that may be attributed to coating surface porosity and soot formation in an engine. Also, some investigators suggest that heat transfer may increase with the higher wall temperatures when the engine is insulated. Another issue is the recent concern that some thermal barrier materials proposed for LHR engines may be partially translucent to thermal radiation from the combustion process of diesel fuels due to soot and particulates formation [2]. It is obvious that the above mechanisms can compromise the insulating effectiveness of the material in reducing the gas-to-wall heat transfer in diesel engines. Computer models have been employed to study the effect of engine operating parameters and configuration on soot formation and radiation heat transfer [3]. However, experimental data are scarce to properly validate these models to predict the effect of fuel composition and combustion geometries that utilize thermal barrier materials with unusual radiative properties.

Another factor is the use of methanol as an alternative fuel for diesel engines which continues to receive increased emphasis due to its potential impact on air quality and petroleum supplies. Again, there is little understanding on how the combustion temperature, heat release rates and emissions of methanol affect the thermal performance of thermal

barrier coatings. In a diesel engine combustion system, the two mechanisms that transfer heat from the flame are convection and radiation. The relative magnitudes of heat transfer by these mechanics vary with flame structure, flame temperature, and fuel composition. For fuels with high carbon to hydrogen ratios, the thermal radiation increases with soot and particulate formation. Unlike diesel fuels, methanol combustion produces non-luminous flames and practically no soot and particulates during combustion. Consequently, the infrared spectral radiation of a methanol flame contains no significant particulate thermal radiation. It is likely, therefore, that the lower thermal radiation generated by methanol and its lower flame temperature due to higher latent cooling effects may have a different impact on the thermal effectiveness of thermal barrier materials as compared to conventional diesel fuels. That is, the most effective thermal barrier for a methanol-fueled engine may not be optimum for a diesel-fueled engine. Based on the mixed results obtained to date and shortcomings in the published data, there is general agreement that a need exists for a better fundamental understanding of the heat transfer in thermal barrier coatings: particularly the effect of surface temperature on in-cylinder heat transfer and thermal radiation on the overall heat transfer. To improve this understanding, an experimental approach is being employed that utilizes bench-type or laboratory rig testing (as a prerequisite to engine testing) for screening the heat transfer effectiveness of thermal barrier coatings when exposed to thermal radiation flux emitted by flames produced by different fuel compositions. In this study a 0.5-mm thick coating of plasma-sprayed zirconia is evaluated with a non-luminous flame (methane) and a luminous flame (n-butane). Gas fuels were used instead of liquid fuels because of simplicity and time constraints. Methane and n-butane were selected because their flame speeds are similar for safe operation in the burner.

2. DESCRIPTION OF TEST APPARATUS

The test apparatus used in the heat transfer evaluation is shown schematically in Fig. 1 and is presented in an overall view in Fig. 2. The apparatus was designed for a nominal heat load of 3 kW and consisted of a pre-mixed burner, a two-piece test section, and a steam generator. Except for the burner, the test apparatus was constructed of stainless steel to minimize compatibility problems. The test section was fabricated to accommodate a disk-shaped test specimen of 70-mm (2.75-in.) diameter and a combined thickness (metal and thermal barrier coating portion) of 13-mm. Heat load to the test section was manually controlled by setting the fuel flow to the burner and adjusting the flame distance with respect to the test specimen in the test section. Heat from the flame passed through the test specimen and was transferred from its upper surface to the steam generator. The boiling process provided temperature stability and uniformity on the upper surface on the specimen.

2.1 BURNER

The pre-mixed burner selected was modified to allow for the metering of air and fuel flow. The burner produced a nominal 6.15 kW (21,000 Btu/h) and 11.72 kW (40,000 Btu/h) of heat with methane and n-butane gas, respectively. Compressed air at 5 psig was required to operate the burner. Grid diameter of the burner was 40-mm (1.50-in.).

2.2 TEST SECTION

The test section consisted of a two-piece cylindrical assembly. Figure 3 shows a view of the test section components. The lower module contained a 76.2-mm (3.00-in.) diameter, 57.2-mm (2.25-in.) long cavity for installation and removal of the 70.0-mm (2.75-in.) diameter test specimen, thus providing a 3.2-mm (0.125-in.) air gap between the test specimen and the

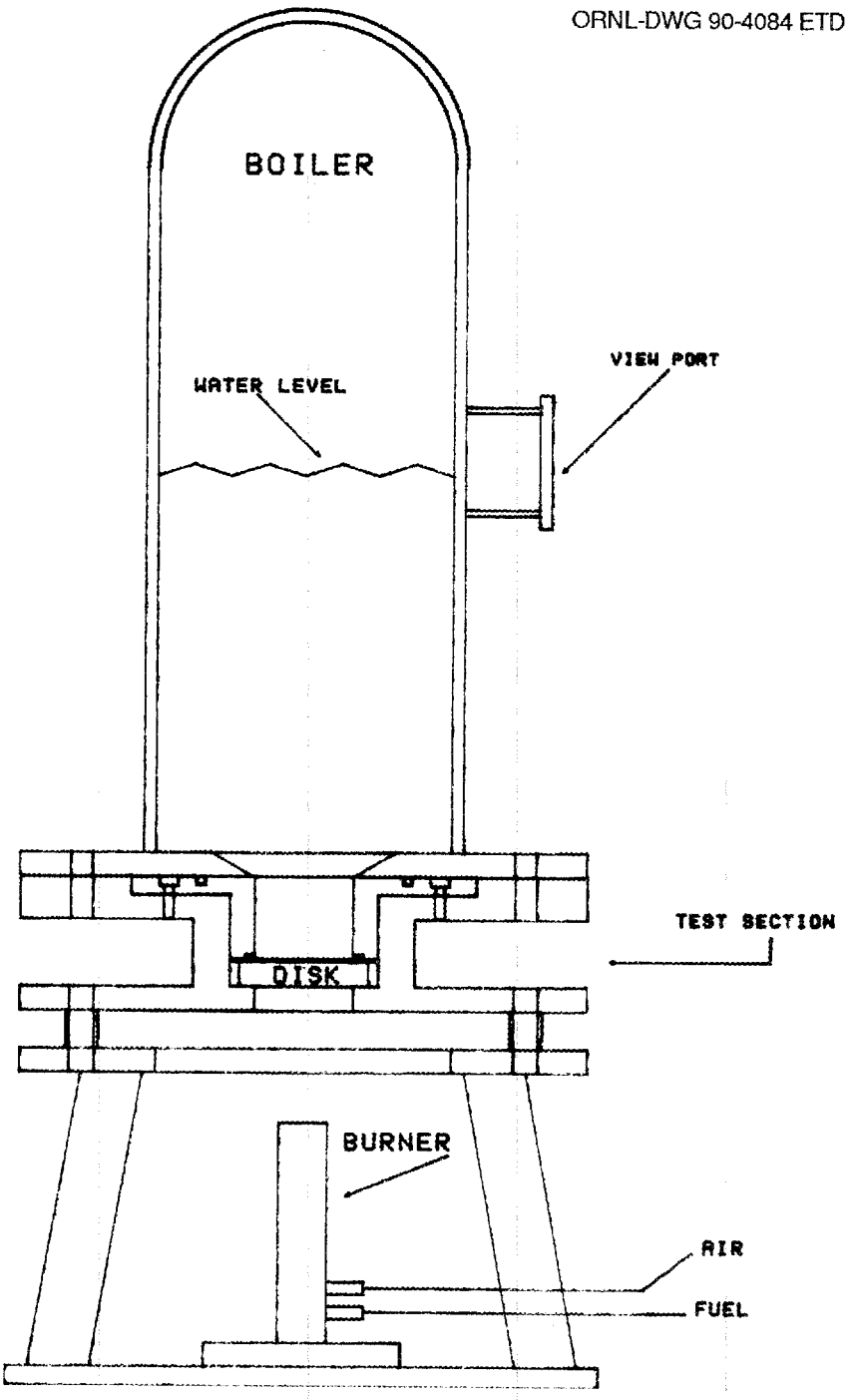

Fig. 1. Schematic of test apparatus.

ORNL PHOTO 8401-90

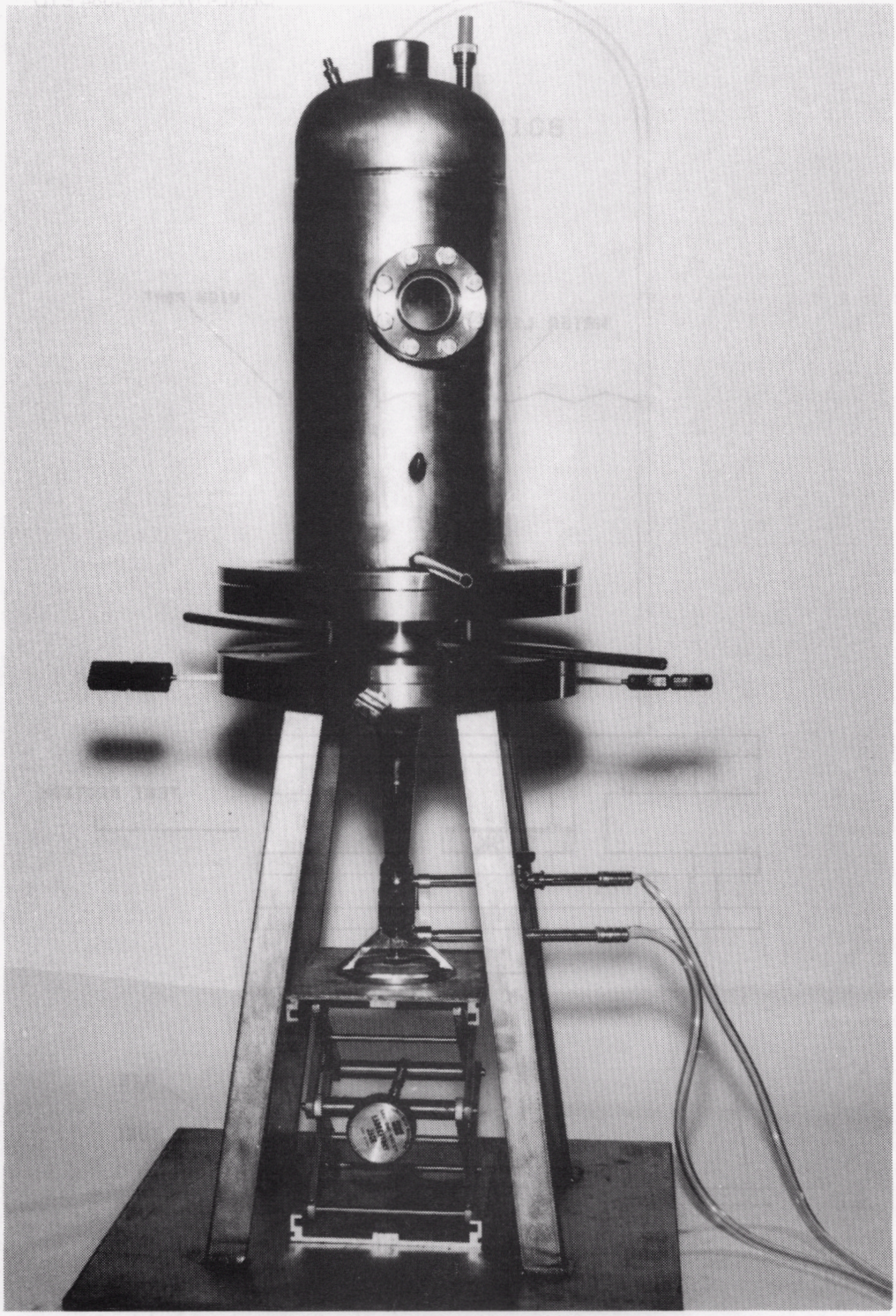

Fig. 2. Photograph of test apparatus.

ORNL PHOTO 8400-90

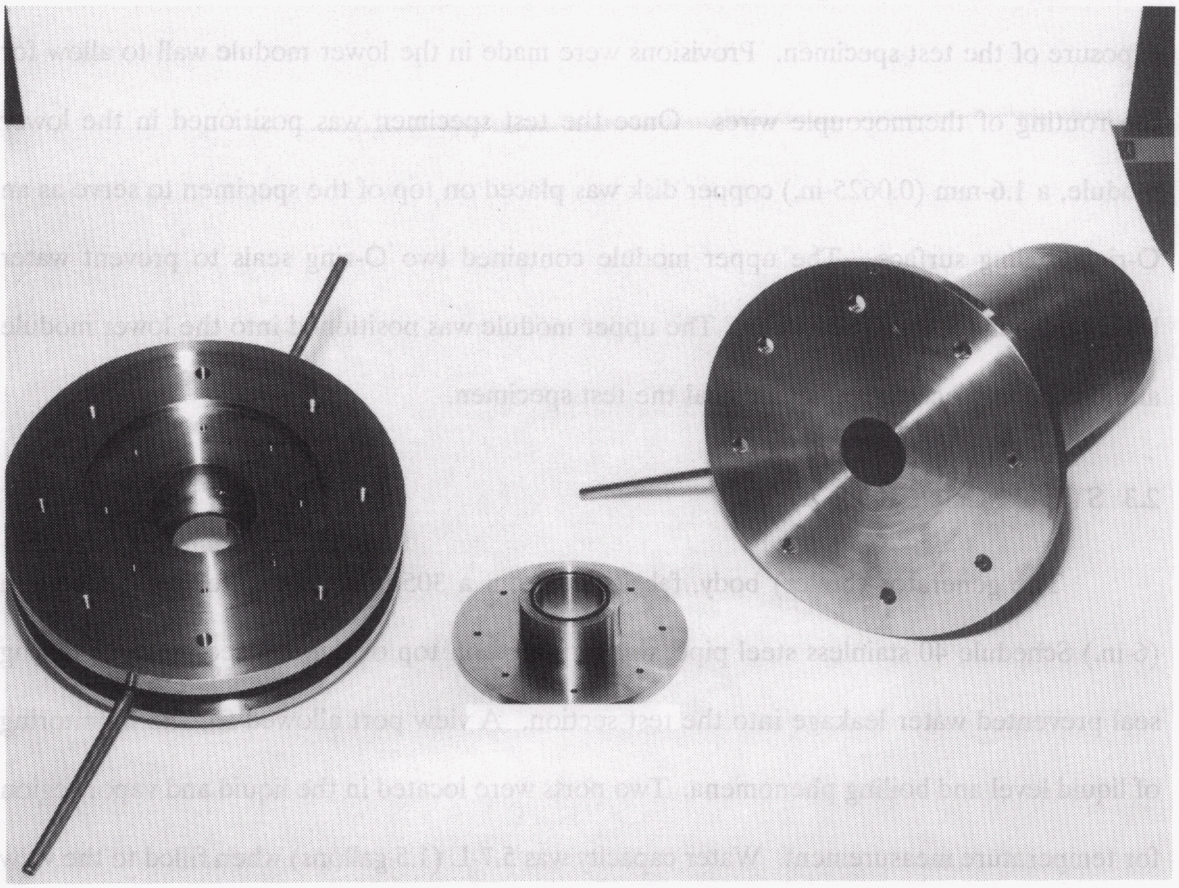

Fig. 3. View of test section components.

test section wall to serve as a resistance to radial heat loss. A 51-mm (2.00-in.) diameter center hole is drilled through the bottom end (flame side) of the lower module to allow flame exposure of the test specimen. Provisions were made in the lower module wall to allow for the routing of thermocouple wires. Once the test specimen was positioned in the lower module, a 1.6-mm (0.0625-in.) copper disk was placed on top of the specimen to serve as an O-ring sealing surface. The upper module contained two O-ring seals to prevent water leakage around the test specimen. The upper module was positioned into the lower module and bolted in place to retain and seal the test specimen.

2.3 STEAM GENERATOR

The generator (boiler) body, fabricated from a 305-mm (12-in.) length of 152-mm (6-in.) Schedule 40 stainless steel pipe, was mounted on top of the test section. An O-ring seal prevented water leakage into the test section. A view port allowed for the monitoring of liquid level and boiling phenomena. Two ports were located in the liquid and vapor region for temperature measurement. Water capacity was 5.7-L (1.5 gallons) when filled to the view port level. Boiling occurred at atmospheric pressure.

3. TEST SPECIMEN

The test specimen consisted of an instrumented, disk-shaped piece of gray cast iron with a 0.5-mm coating thickness of partially stabilized zirconia. The combined (metal and coating) thickness of the test specimen was kept at 13-mm (0.5-in.) to permit proper fit in the test section. The test specimen was fabricated by machining a 70-mm (2.75-in.) diameter disk of gray iron for the corresponding coating thickness. Four thermocouple grooves of 1.6-mm (0.063-in.) depth and width were cut into both the lower and upper surface of the disk. The grooves were machined such that one thermocouple junction could be positioned at the center of the disk and the other three could be positioned along an arc of a 35-mm (1.375-in.) diameter circle, each spaced 120° apart. Figure 4 shows an uncoated gray iron disk with grooves machined for installation of thermocouples. Insulated thermocouple wires were pressed into each groove and routed to the edge of the disk. Thermocouple joints were welded to the surface plane of the gray iron disk. After the installation of thermocouples, the thermal barrier coating was plasma sprayed on one side of the iron disk. The deposited coating was then surface ground to the desired thickness. The final surface finish was 40-50 microns. Figure 5 shows the coated test specimen with the installed thermocouples on the upper (boiling-side) and lower (coating-side) surface. Finally, a thin layer (20-25 microns) of phosphor material was applied to the coating surface for the laser-fluorescence temperature measurement technique as described in Section 4.3. When installed in the test section, the effective diameter of the test specimen exposed to the flame was 50.8-mm (2-in.).

ORNL PHOTO 8403-90

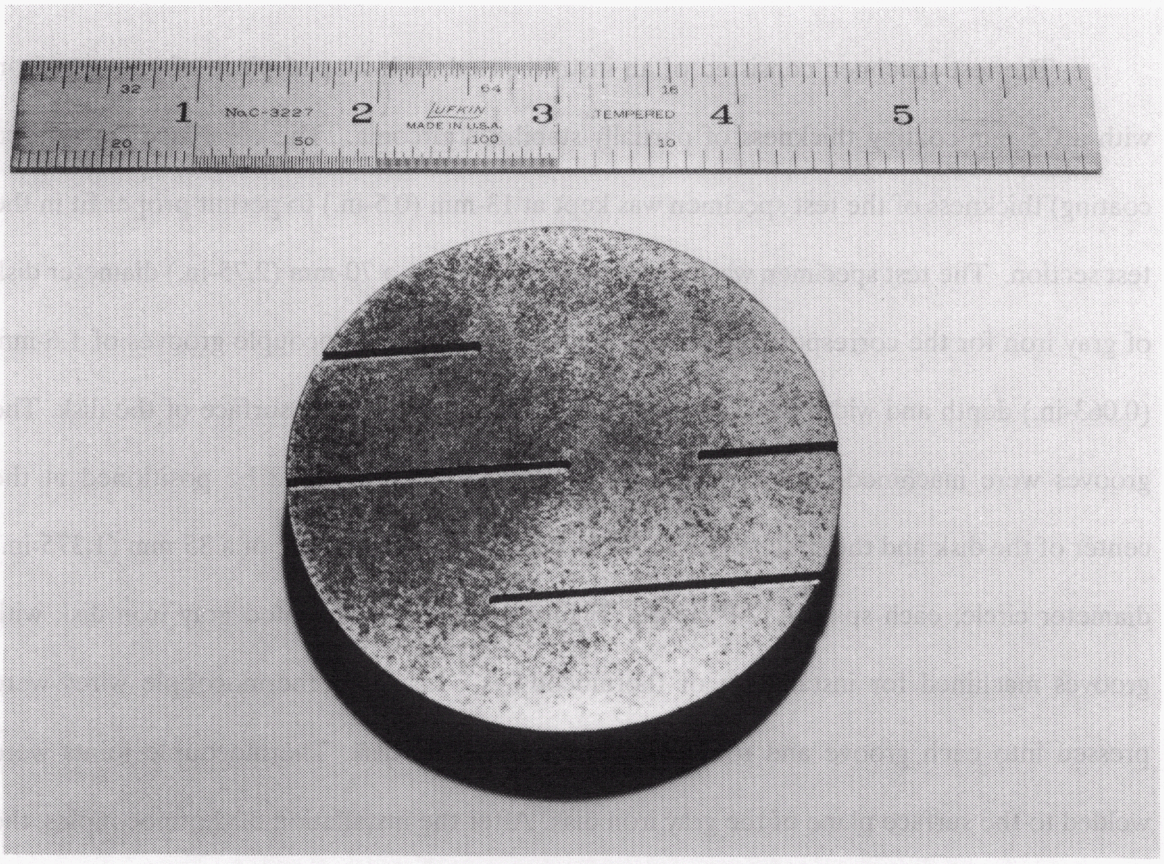

Fig. 4. Photo of uncoated metallic disk with machined grooves.

ORNL PHOTO 6937-90

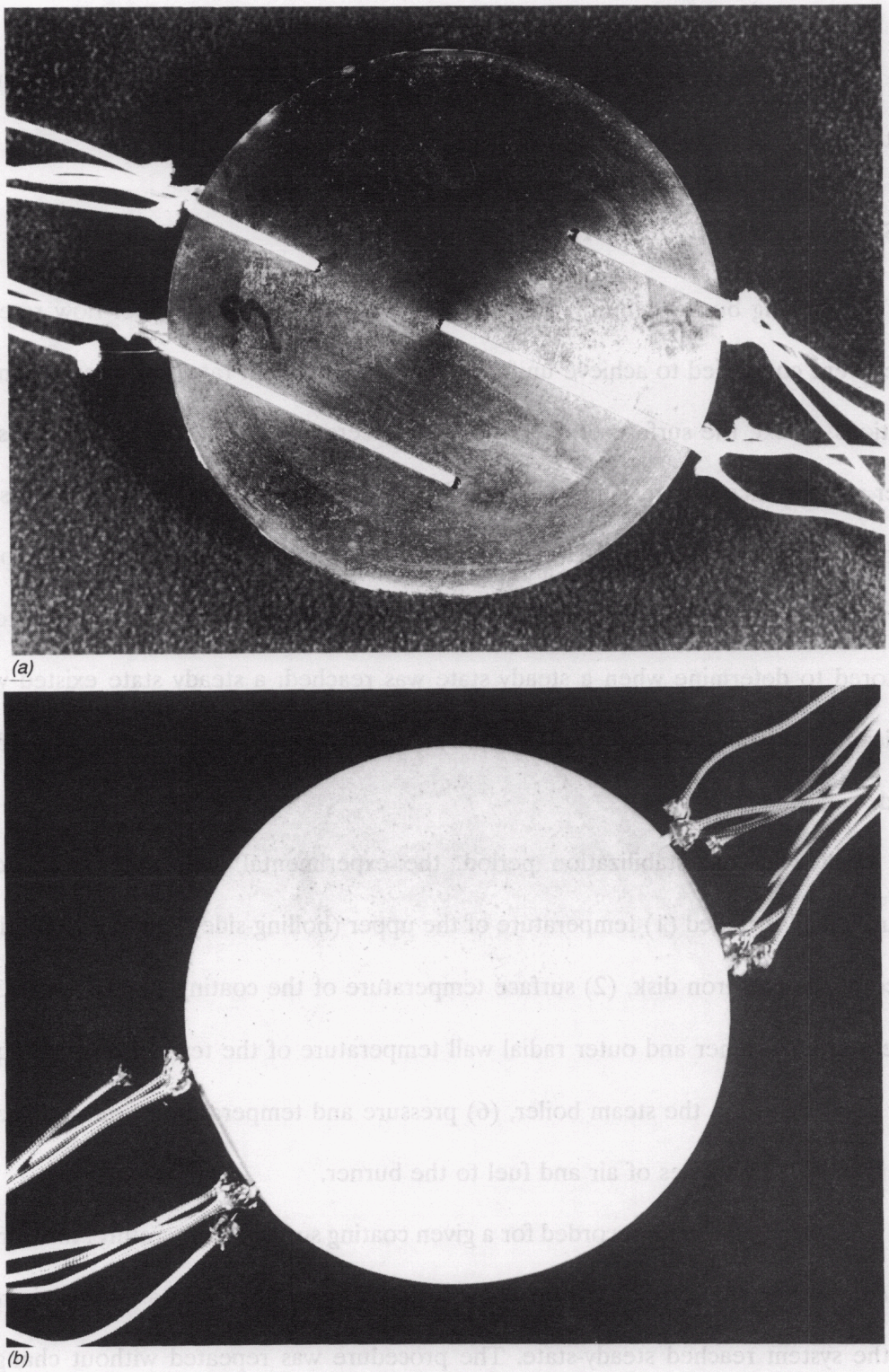

(a)

(b)

Fig. 5. Photo of coated test specimen with installed thermocouples on the boiling-side and flame-side surface.

4. OPERATING PROCEDURE AND INSTRUMENTATION

Heat fluxes, temperature differences, and thermal conductances were calculated from data taken during steady-state operations.

4.1 STEADY-STATE OPERATION

Following burner ignition with a given fuel gas, the air and fuel flow rates to the burner were controlled to achieve uniform flame, desired heat rate, and proper combustion conditions. Next, the surface temperature of the ceramic coating was set by adjusting the burner grid distance with respect to the specimen in the test section. Figure 6 shows the test specimen being heated by a methane flame. The activated fluorescence from the phosphor material can be seen near the coating center. Temperatures throughout the system were monitored to determine when a steady state was reached; a steady state existed when no significant change in temperature (0.5-1.0°C) occurred through the system over a 15 minute period.

Following the stabilization period, the experimental data were recorded. The measured data included (1) temperature of the upper (boiling-side) and lower (coating-side) surface of the cast iron disk, (2) surface temperature of the coating (flame-side), (3) flame temperature, (4) inner and outer radial wall temperature of the test section, (5) liquid and vapor temperature in the steam boiler, (6) pressure and temperature of air and fuel to the burner, and (7) flow rates of air and fuel to the burner.

After the data were recorded for a given coating surface temperature, the burner grid distance was then adjusted to achieve a new surface temperature. Data were again recorded after the system reached steady-state. The procedure was repeated without changing the

ORNL PHOTO 8431-90

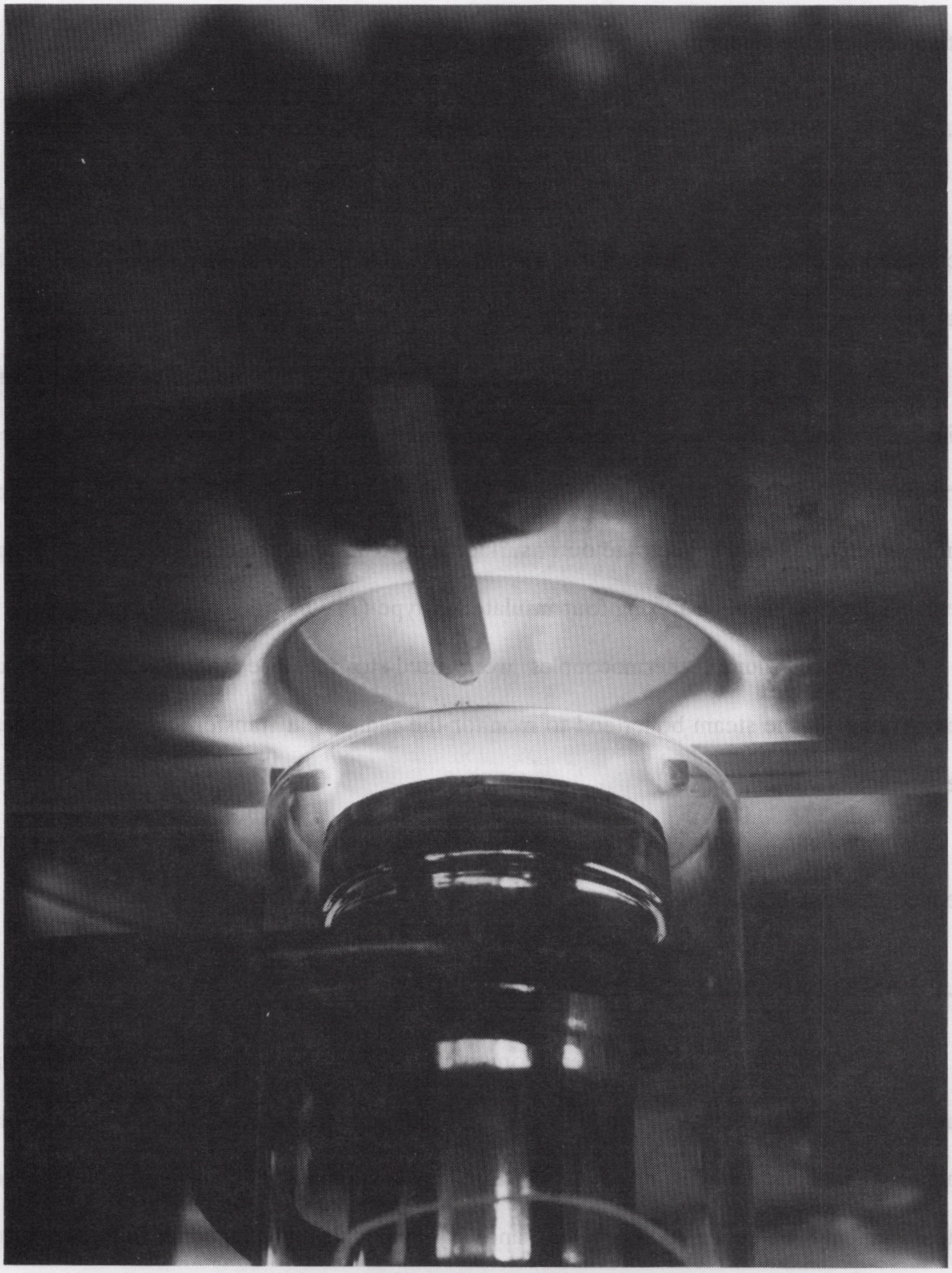

Fig. 6. View of test specimen during exposure to a methane flame.

burner air/fuel setting until heat transfer data were obtained for the thermal barrier coating at various surface temperature for each fuel type.

4.2 INSTRUMENTATION AND DATA ACQUISITION

Fuel and air flow to the burner was measured by rotameters. Pressure and temperature of the fuel and air were also measured. The above information was used to calculate burner heat rate.

Platinum-platinum/13% rhodium (Pt-Pt/13% Rh) thermocouples, of 0.010-in. wire diameter, were used to measure the upper and lower metal surface temperature of the test specimen. Four thermocouples were installed on each surface of the disk. Laser-fluorescence thermometry was used to measure outer surface temperature of the ceramic coating. Flame temperature was measured using four insulated R-type (Pt-Pt/13% Rh) thermocouples.

Chromel-Alumel thermocouples were used to measure the liquid and vapor temperature in the steam boiler and to monitor the radial heat transfer loss across the test section wall.

An Acurex Autodata Ten/10 datalogger was used to provide data collection and reduction capabilities.

4.3 LASER-FLUORESCENCE THERMOMETRY

Some attributes of the laser-fluorescence technique over conventional thin-film thermocouple or pyrometric methods include (1) immunity to surface emissivity and thermal radiation background, (2) remote, non-contact application, (3) absolute temperature measurement (no reference required) and (4) avoidance of junctions and lead wires complexities through ceramic coating.

The use of laser-fluorescence thermometry to obtain high temperature measurements on surfaces has been described in previous reports [4,5]. The technique involves the pulsed activation of a thin layer of a chemically stable, rare-earth-doped phosphor material that exhibits a strong fluorescence behavior with absolute temperature. The surface painted phosphor is activated by using a laser system which produces nanosecond-duration pulses in a variety of ultraviolet (UV) wavelengths. A calibration curve is generated for the phosphor by recording the characteristic decay of fluorescent emission bands during its activation by pulsed UV wavelengths as a function of absolute temperature. A measure of component surface temperature is obtained from the calibration curve by measuring the decay time of fluorescence intensity of the phosphor at the surface. Figure 7 taken from Ref. 4 shows the laser-induced fluorescence lifetimes of several rare-earth doped, phosphor materials. A linear behavior is noted for the decay lifetimes of several phosphors when they are excited at high temperatures.

The phosphor applied to the ceramic coating in this study was a mix of 50% manganese-doped, magnesium fluorogermanate [$Mg_4(F)GeO_6$:Mn] and 50% europium-doped, yttrium oxide (Y_20_3:Eu) powder. This combination allowed the capability to measure a temperature range from 400° to 900°C. Figure 8 shows the calibration curve for this phosphor. A high temperature binder was used in the mixture to allow deposition of the phosphor on the surface.

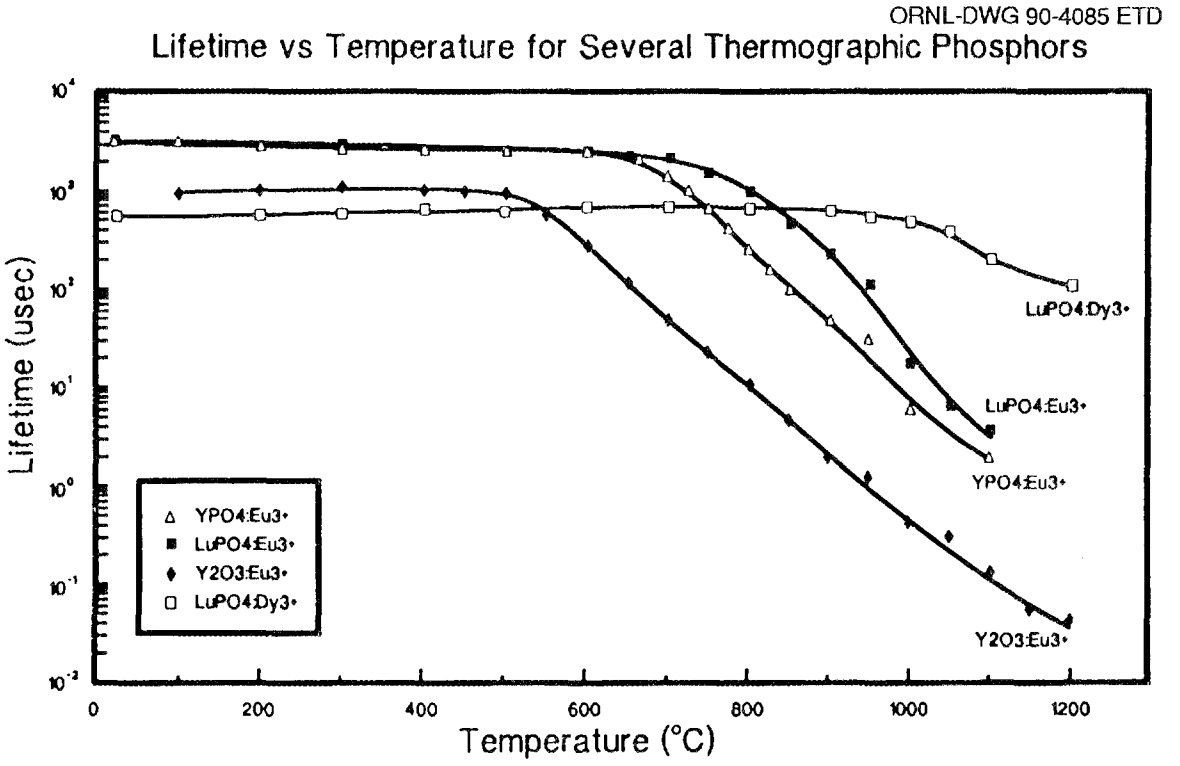

Fig. 7. Laser-induced fluorescence lifetimes of several rare-earth doped phosphor-materials.

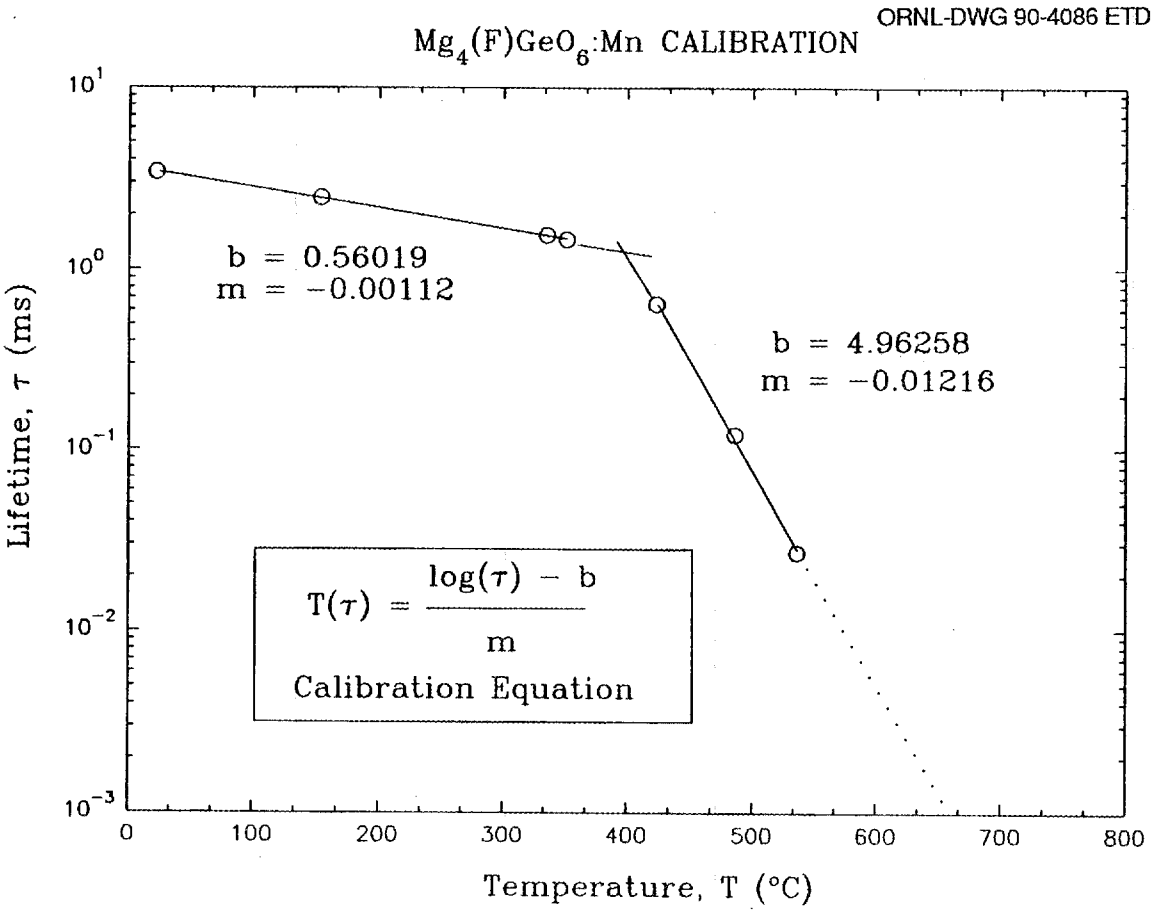

Fig. 8. Calibration curve for 50% Mg_4FGeO_6:Mn and 50% Y_2O_3:Eu phosphor.

5. CHARACTERISTICS OF GRAY CAST IRON AND THERMAL BARRIER COATING IN TEST SPECIMEN

The gray cast iron material used in the construction of the test specimen was provided by Cummins Engine Company, Inc., and Caterpillar, Inc. The thermal conductivity of the gray iron material in the test specimen was required to calculate the heat flux through the thermal barrier coating. Since no thermal conductivity data were made available by the engine manufacturers, it became necessary to determine these data for the temperature range of interest. Table 1 lists the chemical composition of the cast iron material used.

Table 1. Gray cast iron chemical composition

Element	% Volume
Carbon	3.43
Silicon	2.00
Manganese	0.59
Phosphorus	0.03
Copper	0.55
Molybdenum	0.25
Aluminum	0.009
Nickel	0.09
Tin	0.01
Sulfur	0.10
Chromium	0.26
Carbon Equivalent[a]	4.10

[a]Carbon equivalent is calculated as percentage carbon plus 0.3 times the sum of percentage silicon and phosphorus.

It should be noted that the thermal conductivity of gray irons can be influenced by their chemical composition. High silicon, nickel, and aluminum contents lower the thermal conductivity markedly, whereas phosphorus and manganese reduce the thermal conductivity slightly.

The thermal conductivity data were generated by the ORNL High Temperature Materials Lab (HTML) from the product of thermal diffusivity, density, and specific heat. A laser-flash diffusivity apparatus was used to measure thermal diffusivity data from 170° to 425°C. A Stanton-Redcroft Differential Scanning Calorimeter was used to measure specific heat from 100° to 500°C. The density was calculated from sample weight and volume. Actual thermal diffusivity data and calculated density were combined with the second order polynomial fit to the specific heat data to obtain thermal conductivity values from 175° to 475°C. These values along with a polynomial fit of the data are shown in Fig. 9. All thermal conductivity values fell within 3% of the curve fit as shown in Fig. 10.

The composition of partially stabilized zirconia powder used for the ceramic coat consisted of 95% wt ZrO_2 and 5% wt CaO as the stabilizer. Property data for the powder are listed in Table 2. This powder was selected because it was readily available at ORNL. The plasma spray deposition was conducted at ORNL to maximize quality control in the overall fabrication of the test specimen.

Table 2. Spray powder property data

Composition (% wt:):	ZrO_2 = 95.0 CaO = 5.0
Particle Size:	–200 + 325 mesh (74-44 μm)
Density:	5.7 g/cm^3

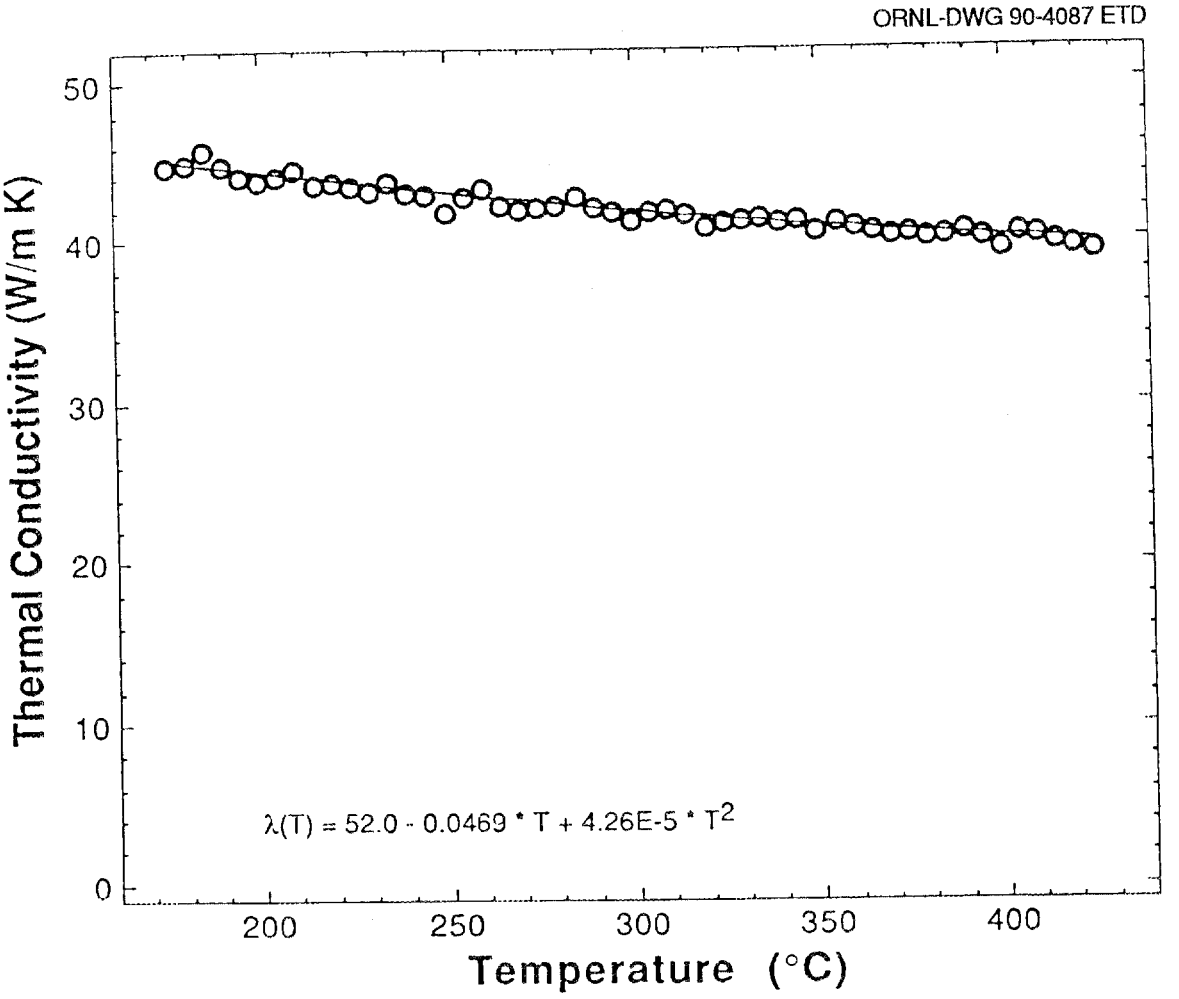

Fig. 9. Thermal conductivity of gray cast Iron.

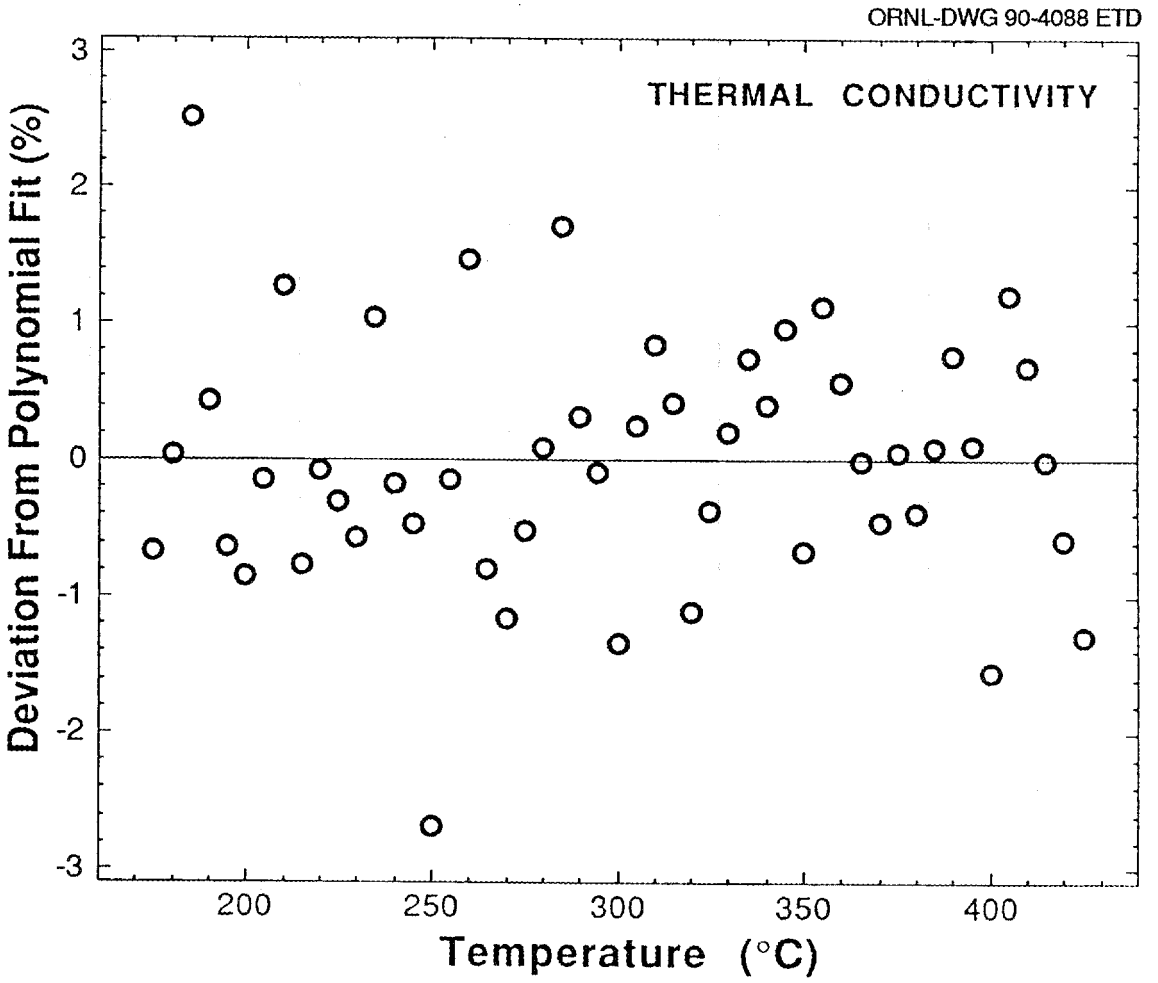

Fig. 10. Percent deviation of thermal conductivity of gray iron.

6. TEST PLAN

To determine the effect of fuel composition and temperature on the heat transfer effectiveness of the thermal barrier coating it was proposed to run tests over a wide range of surface temperatures that may be typically encountered in a diesel engine combustion chamber wall. For each fuel used, the heat flux, temperature gradient, and composite thermal conductance for the coating would be calculated over a 400° to 900°C temperature range. Unfortunately, it was not possible to achieve surface temperatures above 300°C with the existing burner. Therefore, all heat transfer data presented in this study were taken below the surface temperature range originally proposed.

7. HEAT TRANSFER ANALYSIS

Heat flow from the flame through the test specimen to the steam boiler was assumed to be one-dimensional. Although flame temperature was measured in this study, no attempt was made to determine the convective and radiative flux produced by the flame. Only heat transfer through the test specimen was considered. The method used to reduce the data is as follows:

The overall heat transfer conductance in the test specimen (metal and coating) is given by:

$$U = \frac{Q}{A\,\overline{\Delta T}} \quad , \tag{7.1}$$

where $\overline{\Delta T}$ is the overall temperature difference between the flame-side surface of the coating and boiling-side surface of the gray iron disk, and Q/A is the heat flux across the test specimen. The surface temperature of the iron disk is based on an average of four thermocouple readings.

The heat flux is calculated from the conduction heat transfer through the gray iron material according to the relation

$$\frac{Q}{A} = k_m \frac{\Delta T_m}{\Delta X_m} \quad , \tag{7.2}$$

where ΔT_m is the temperature difference of the metallic portion, k_m is the thermal conductivity of the gray iron taken from Fig. 9 and evaluated at the arithmetic mean temperature of the gray iron, and ΔX_m is the gray iron thickness.

The overall resistance (or inverse conductance) to heat flow in the test specimen is equal to the sum of individual resistances ($1/U = \Sigma R$). For the metallic portion of the test specimen the thermal resistance is based on conductive heat flow. Since the coating is assumed to be semi-transparent, its thermal resistance is based on parallel-connected conductive and radiative heat flow paths. If surface fouling is neglected, the overall resistance for the test specimen can be represented as:

$$\frac{1}{U} = (R_{cond})_{metal} + \left[\frac{R_{cond}\, R_{rad}}{R_{cond} + R_{rad}}\right]_{coating} . \tag{7.3}$$

The parallel-connected resistance for the coating is defined as a "composite" resistance ($1/h^*$); therefore,

$$\frac{1}{h^*} = \frac{R_{cond}\, R_{rad}}{R_{cond} + R_{rad}} . \tag{7.4}$$

Substituting Eq. (7.4) into Eq. (7.3) and rearranging, the composite resistance becomes:

$$\frac{1}{h^*} = \frac{1}{U} - (R_{cond})_{metal} . \tag{7.5}$$

Introducing individual heat transfer conductances, the composite resistance for the coating can be expressed as:

$$\frac{1}{h^*} = \frac{\dfrac{\Delta X_c}{h_r\, k_c}}{\dfrac{1}{h_r} + \dfrac{\Delta X_c}{k_c}} , \tag{7.6}$$

where h_r is the radiative heat transfer conductance for the coating, k_c is the thermal conductivity (without radiative component) of the coating, and ΔX_c is the coating thickness.

Rearranging Eq. (7.5), the composite conductance h^* for the coating can be calculated from:

$$h^* = \frac{1}{\frac{1}{U} - \frac{\Delta X_m}{k_m}} \quad . \tag{7.7}$$

Once h^* is known, the radiative heat transfer conductance for the coating can be calculated using a rearranged form of Eq. (7.6):

$$h_r = h^* - \frac{k_c}{\Delta X_c} \quad . \tag{7.8}$$

Equation (7.8) requires that the thermal conductivity of the coating in the absence of direct radiant transmission be known for a given temperature of the material. To evaluate the thermal conductivity of the coating, tests at low surface temperatures are required to avoid high temperature and thermal radiation effects through the coating. The thermal conductivity data obtained for the coating can then be extrapolated to higher temperatures for use in Eq. (7.8) to obtain h_r. However, as pointed out in the previous section, it was not possible to operate at high surface temperatures due to burner limitations. This setback prevented the determination of the radiative heat transfer conductance for the coating via Eq. (7.8).

8. RESULTS AND DISCUSSION

Figures 11 and 12 show the heat transfer results obtained on a 0.5-mm thick, plasma-sprayed, CaO-stabilized, ZrO_2 coating when heated by a methane and n-butane flame. Figure 11 compares the composite (combined conduction and radiation resistance) of the material as a function of mean temperature. Figure 12 presents the thermal conductance on a heat flux basis. Figures 11 and 12 show data from two sets of runs made with each fuel. As shown in Fig. 11, the thermal conductance data were taken over the temperature range of 173°-240°C (446-513 K). Due to burner problems and limitations it was not possible to obtain information over the wider range of temperatures planned (400°-900°C) to determine significant heat transfer effects and make any comparison on the trends with respect to higher temperatures. Also, it was difficult to obtain data with the two fuels over the same temperature range for a good comparison. Surprisingly, although measured flame temperatures for both fuels ranged from 850° to 950°C, the highest surface temperature measured on the coating was 291°C at a constant temperature heat sink of 100°C. One possible explanation for this occurrence is that the convective heat flux from the flame to the coating was seriously reduced by operating with an open flame. Another problem encountered was the difficulty in reducing the amount of premixed air on the burner to produce a reasonable luminous flame with n-butane.

The limited experimental data presented in Figs. 11 and 12 are averaged values of back-to-back, steady state data points obtained for the same run. This was done to increase the experimental accuracy associated with the laser-fluorescence measurement of coating surface temperature. As was stated in Section 4.3, the combined phosphor materials applied to the coating were selected to allow measurement over the 400°-900°C temperature range. Unfortunately, below 300°C, the slope of decay time versus temperature for magnesium

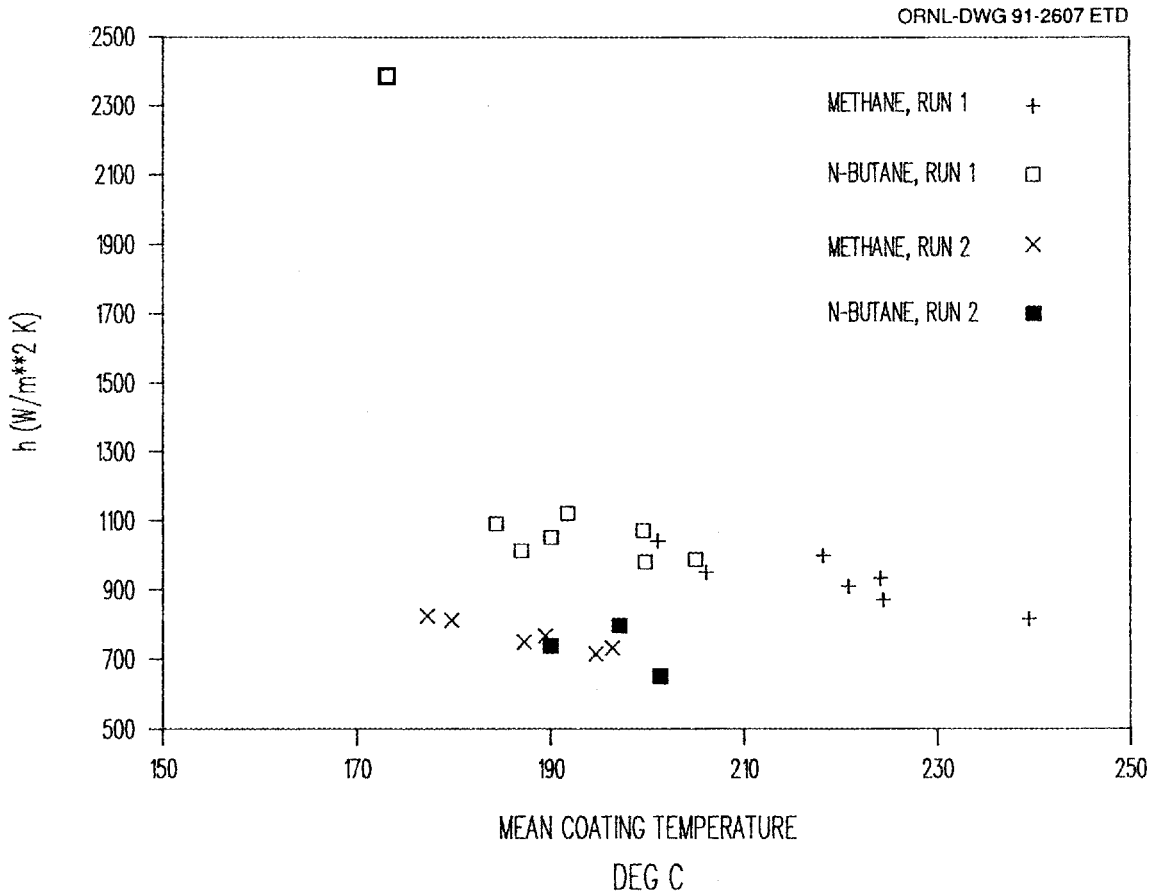

Fig. 11. Composite thermal conductance of plasma-sprayed Z_rO_2 as a function of temperature obtained with methane and n-butane flames.

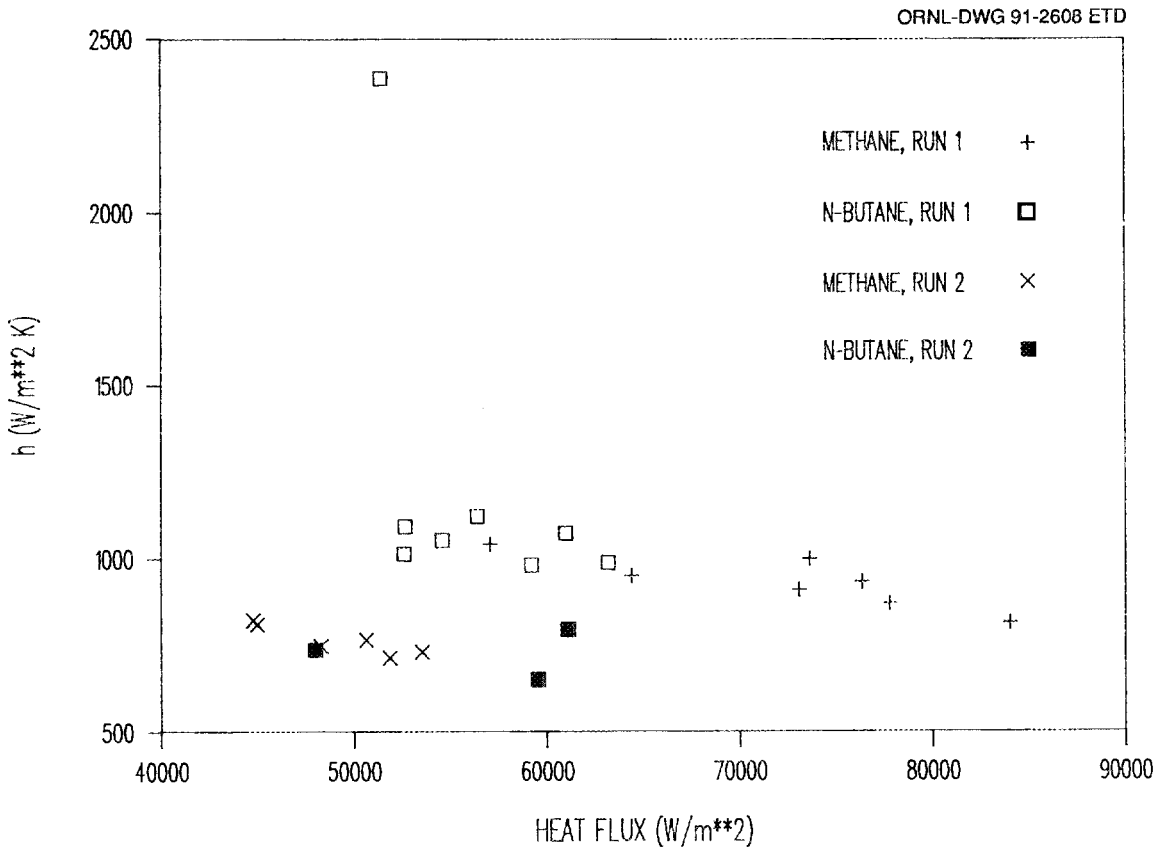

Fig. 12. Composite thermal conductance of plasma-spray Z_rO_2 as a function of heat flux obtained with methane and n-butane flames.

fluorogermanate can yield a greater difference in temperature for a small change in decay time. The uncertainty in temperature measurement that may have resulted from this situation was reduced by taking the average of two steady state points at the same operating condition. Overall, the laser-fluorescence method yielded good results in the presence of radiant flames.

The results shown in Fig. 11 indicate that the thermal conductance of the coating not only varied with temperature, but decreased after reheating the coating (Run 2 tests) with either a methane or n-butane flame. For the Run 1 tests, the composite conductance ranged between 2386 and 816 $W/m^2 \bullet K$ (1.19-41.0 $W/m \bullet K$ for 0.5-mm coating) over the 173°-240°C temperature range covered. The heat flux range corresponding to this conductance range was 51.4-84.0 kW/m^2 as indicated in Fig. 12. In Fig. 11, data obtained with n-butane heating during Run 1 test show a dramatic decrease in thermal conductance over a very narrow temperature range. From 173° to 184°C, the thermal conductance decreased by 54% (2386 to 1091 $W/m^2 \bullet K$, respectively). It is not known whether a similar decrease can be expected with methane since data for this fuel could not be obtained in this temperature range during Run 1 tests. Figure 12 shows the same behavior on a heat flux basis.

Run 2 tests were conducted primarily to confirm some of the results noted during early heat transfer tests, particularly in the 173° to 184°C temperature range. Surprisingly, the reheat results presented in Figs. 11 and 12 show an apparent degradation in thermal conductance for the ceramic coating evaluated. No significant difference in thermal performance is noted between methane and n-butane reheating. At a mean temperature of 200°C, Fig. 11 illustrates the thermal conductance from Run 2 tests to be 30% below Run 1 results.

Thermal barrier materials that exhibit temperature dependent thermal properties as well as irreversible changes with reheating can adversely effect diesel engine performance. In

an IC engine the gas-to-wall heat transfer near the combustion chamber wall is highly transient. This cyclic heat exchange produces surface temperature swings which impact engine thermal performance, component thermal stresses, and lubricating efficiency during the cycle. When applied in a combustion chamber, a temperature dependent coating can have an effect on the transient heat transfer by influencing the gas-to-wall temperature dynamics and surface temperature swings. For the range of temperature covered it is difficult to determine from the scatter of the data any effects or establish any trends on thermal barrier heat transfer due to flame luminosity. This is probably due to the problems discussed earlier, i.e. lower operating temperatures and inadequate flame luminosity with n-butane due to poor air-fuel ratio control. However, a thermal barrier material that is translucent would allow radiation heat flux from the flame to pass through and be deposited on the metal substrate, thus raising the metal temperature. Examination of the experimental data did not indicate a temperature shift on the substrate surface in the test specimen between the methane and n-butane case at similar heat flux. From this observation, it is believed that the amount of radiative flux transmitted through the coating during low temperature operation was neglibible.

The thermal conductance of 816 $W/m^2 \bullet K$ given in Fig. 11 at a mean temperature of 240°C (513 K) is in good agreement with the results of Wilkes and Lagerdrost [6] for CaO-stabilized zirconia. In their study, the thermal conductivity of plasma-sprayed zirconia calculated from thermal diffusivity measurements was 0.45 $W/m \bullet K$ at 600 K in a vacuum. This agrees well with the 0.41 $W/m \bullet K$ value obtained when the thermal conductance of 816 $W/m^2 \bullet K$ is multiplied by the 0.5-mm coating thickness tested. Brandt [7] reported thermal diffusivity measurements of zirconia coatings stabilized with 8% CaO in a vacuum that gave an equivalent thermal conductivity of 0.5 $W/m \bullet K$ in the temperature range of 700-

1300 K. However, both sets of experimental data [6,7] show large irreversible increases in thermal conductivity after heating the coating to temperatures above 1300 K. This increase in thermal conductivity is explained by changes in the material's pore morphology. At low temperatures (<1000 K) the thermal conductivity of the pore phase is small. At elevated temperatures (>1000 K) the radiative heat transfer across the pores become significant which increases the composite (conductive plus radiative) thermal conductivity. Also, if the material is translucent to thermal radiation at some wavelengths, the composite conductivity is likely to increase even further. In summary, the results obtained by Wilkes and Lagerdrost [6] and Brandt [7] suggest that high temperatures (>1300 K) make the thermal conductivity of plasma-sprayed zirconia go up. We found in this study that the thermal conductivity decreased irreversibly after mild heating. Due to limitations in operating temperature levels, it was not possible to confirm any trends toward increased thermal conductance with respect to high temperature.

9. CONCLUSIONS

The purpose of this experimental effort was to provide a screening tool for ranking candidate thermal barrier materials for use in alternative-fueled and diesel-fueled engines.

A test apparatus was fabricated and used to evaluate the heat transfer effectiveness of a 0.5-mm thick, plasma-sprayed, CaO-stabilized, zirconia coating when heated by a non luminous (less radiant) and luminous flame. A laser-fluorescence method used to measure coating surface temperature yielded good results in the presence of radiant flames.

Due to burner limitations, it was not possible to obtain data over a wide temperature range to determine significant heat transfer effects or trends toward increased thermal conductance with respect to decreased temperature. Also, it was difficult to make any comparison on thermal barrier heat transfer trends with flame luminosity due to poor air-fuel ratio control. Within the temperature range of 173°-240°C (446-513 K), the results showed that the thermal conductance decreased by 66% with temperature. At 513 K the value obtained for thermal conductance agreed fairly well with reported experimental values obtained in a vacuum at about 600 K. For n-butane flame heating, the thermal conductance of the coating decreased by 54% over a very narrow temperature range. Reheating of the coating produced an apparent irreversible change in thermal conductivity. The thermal conductance was reduced an additional 30% for a given temperature following reheating with both fuels. No significant difference in thermal conductance was noted between methane and n-butane reheating. The use of thermal barrier materials that exhibit modest temperature dependent thermal conductance and irreversible changes in heat transfer effectiveness with reheating can influence the gas-to-wall temperature dynamics, surface temperature swing, and net heat flux in the combustion chamber of a diesel engine and affect its operating performance component life, and lubricating efficiency.

10. FUTURE WORK

As a result of problems encountered during operation of the test apparatus, several recommendations for future work to improve accuracy and operating temperature range appear warranted. They are as follows:

1. A new burner system should be sized and designed to provide a wider flame temperature range and permit sufficient variations in air-fuel ratio to produce various flame luminosities for a given fuel. The burner should operate on methanol and diesel fuel to better approximate fuel conditions in an engine.
2. A mono-chromator and associated equipment should be installed to measure the infrared radiation spectra from the flame.
3. A calibration check should be performed on the test apparatus using a well characterized reference material. The thermal conductivity of such material should be measured over a temperature range similar to that anticipated for the thermal barrier coating and compared to the reference value.
4. A different phosphor material for laser thermometry measurements should be used on a coating for operation below 400°C.

Following the incorporation of the above recommendations, future test work will involve steady-state as well as transient heat transfer measurements of candidate thermal barrier materials over a temperature range of 400°-1000°C in order to determine the temperature and thermal radiation dependence on the composite thermal conductivity with diesel and methanol fuels. Irreversible changes in thermal performance with reheating will also be investigated.

ACKNOWLEDGEMENTS

This work was performed at Oak Ridge National Laboratory for the U.S. Department of Energy (DOE), Office of Propulsion Systems and Office of Alternative Fuels. John W. Fairbanks served as program manager for DOE under the Heavy Duty Transport Technology Program.

The author appreciates the assistance of many ORNL staff members and is particularly grateful for the contributions of R. L. Graves, group leader, Engineering Technology Division; E. L. Biddle, engineer technologist, for assistance in the installation of the test equipment; R. S. Graves, Metals and Ceramics Division, for the instrumentation of test specimens; M. L. Santella, Metals and Ceramics Division, for plasma spraying the test specimens; C. Hubbard, Metals and Ceramics Division, for the thermal characterization of gray iron material; and M. R. Cates, D. L. Beshears, and S. W. Allison, of the Applied Technology Division for their support in the installation and operation of the laser thermometry equipment to measure coating surface temperature.

REFERENCES

1. C. S. Reddy, N. Domingo, and R. L. Graves, *Low Heat Rejection Engine Research Status: Where Do We Go From Here?* SAE Paper No. 900620, 1990 .
2. S. Wahiduzzaman and T. Morel, *Effect of Ceramics Translucence on Heat Barrier Effectiveness in Diesel Engines*, SAE 890569, 1989.
3. T. Morel, R. Keribar, *Heat Radiation in D.I. Diesel Engines*, SAE 860445, 1986.
4. S. W. Allison and M. R. Cates, *Solid-State Fluorescence Above 1000°C, Applications to High-Temperature Laser Thermometry*, ORNL/ATD-21, January 1990.
5. S. W. Allison, et al., *Sensing Applications of Rare-Earth Doped Luminescent Materials*, ORNL/ATD-10, April 1989.
6. K. E. Wilkes and J. F. Lagerdrost, NASA Contract Report CR-121144, 1573.
7. R. Brandt, High Temperature, High Pressure, 13 (1981) 79.

INTERNAL DISTRIBUTION

1. S. W. Allison
2. R. L. Beatty
3. D. L. Beshears
4. P. J. Blau
5. R. A. Bradley
6. C. R. Brinkman
7. R. S. Carlsmith
8. M. R. Cates
9. J. C. Conklin
10. D. H. Cook
11. W. G. Craddick
12. R. M. Davis
13–22. N. Domingo
23. E. C. Fox
24. W. Fulkerson
25. R. L. Graves
26. R. S. Graves
27. C. Hubbard
28. D. R. Johnson
29. J. E. Jones Jr.
30. T. S. Kress
31. T. G. Kollie
32. E. L. Long, Jr.
33. R. N. McGill
34. M. W. Rosenthal
35. M. L. Santella
36. A. C. Schaffhauser
37. V. J. Tennery
38. B. H. West
39. R. K. Williams
40. Central Research Library
41–42. Laboratory Records Department
43. Laboratory Records, ORNL RC
44. ORNL Patent Section
45. Technical Library Y-12, DRS

EXTERNAL DISTRIBUTION

46. Alex C. Alkidas, GM Research Labs., Warren, MI 48090-9055
47. Richard L. Allor, Ford Motor Company, Materials Systems Reliability Division, 20000 Rotunda Drive, P.O. Box 2053, Dearborn, MI 48121-2053
48. R. T. Alpaugh, DOE, Office of Transportation Systems, CE-151, Forrestal Bldg., 1000 Independence Ave., Washington, D.C. 20585
49. C. A. Amann, GM Research Labs, Engine Research Department, Warren, MI 48090
50. Dennis N. Assanis, Department of Mechanical and Industrial Engineering, University of Illinois-Urbana, 1206 West Green St. Urbana, IL 61801
51. John M. Bailey, Caterpillar Tractor Company, Research Department, Technical Center, P.O. Box 1875, Peoria, IL 61629
52. M. M. Bailey, NASA Lewis Research Center, MS 86-6, 21000 Brookpark Road, Cleveland, OH 44135
53. R. F. Barrows, NASA Lewis Research Center, MS 86-6, 21000 Brookpark Road, Cleveland, OH 44135
54. J. A. Bledsoe, General Electric Company, Bldg. 7, Advanced Energy Program Department, P.O. Box 527, King of Prussia, PA 19406
55. Paul N. Blumberg, Ricardo-ITI, 645 Blackhawk Drive, Westmont, IL 60559
56. D. J. Boes, Westinghouse Electric Corporation, R&D Center, 1310 Beulah Road, Pittsburgh, PA 15235
57. G. L. Borman, Professor, University of Wisconsin-Madison, 1500 Johnson Drive, #119, Madison , WI 53706

58. Michael Brands, Cummins Engine Company, P.O. Box 3005, Columbus, IN 47201
59. J. J. Brogan, DOE, Office of Propulsion Systems, Forrestal Bldg., CE-32, Washington, DC 20585
60. W. Bryzik, (AMSTA-RGR), U. S. Army TACOM, 11 Mile Road, Warren, MI 48397-5000
61. Enrico J. Caruso, White Engines, Inc., Vice President, Engineering, Canton, OH 44707
62. A.A. Chesnes, DOE, Office of Transportation Technologies, Forrestal Bldg., CE-30 Washington, DC 20585
63. Dr. Charles Church, HQDA (DAMA-ARA), Washington, D.C. 20310
64. Richard Chute, Eaton Corporation, Engine and Research Center, 26201 Northwestern Highway, P.O. Box 766, Southfield, MI 48037
65. Harry E. Cook, Chryslet Motors Corporation, Automotive Research and Technical Planning, 1200 Chrysler Drive, Highland Park, MI 48288-1118
66. R. G. Colello, A.D. Little, Inc., Acorn Park, Cambridge, MA 02140
67. W. J. Croft, U.S. Army Materials Technology Laboratory, 405 Arsenal Street, Watertown, MA 02172
68. Davis Dimick, Advanced Product Engineering, GM Technical Center, Warren, MI 48090
69. M. Dowdy, JPL, 4800 Oak Grove Drive, Pasadena, CA 91103
70. Dr. V.K. Duggal, Cummins Engine Company, MS-50165, P.O. Box 3005, Columbus, IN 47202
71. N. Richard Dunteman, Electromotive Division, General Motors Corp., LaGrange, IL 60525
72. Dr. T. Michael Dyer, Combustion Applications Division, Sandia National Laboratories, Livermore, CA 94550
73. J. J. Eberhart, DOE, Office of Transportation Materials, Forrestal Bldg., CE-34, Washignton, D.C. 20585
74. J. J. Egan, International Harvester, 10400 W. N. Avenue, Melrose Park, IL 60160
75. R. C. Evans, NASA Lewis Research Center, 21000 Brookpark Road, MS 86-6, Cleveland, OH 44135
76. John. W. Fairbanks, DOE, Heat Engine Propulsion Division, Forrestal Bldg., CE-322, Washington, D.C. 20585
77. R. D. Fleming, EFE Consulting Services, 17508 Clinton Drive, Accokeek, MD 20607
78. George E. Gazza, U. S. Army Materials Technology Laboratory, Ceramics Research Division, 405 Arsenal Street, Watertown, MA 02172
79. P. C. Glance, Concept Analysis Corporation, 950 Stephenson Highway, Dupont Automotive Development Bldg., Troy, MI 48007-7013
80. Robert J. Gottschall, DOE, Office of Material Sciences, ER-131 GTN, MS:G-256, Germantown, MD 20545
81. Marvin Gunn, DOE, Advanced Industrial Concepts Division, Forrestal Bldg., CE-232, 1000 Independence Avenue SW, Washington, D.C. 20585

82. Nabil Hakim, Detroit Diesel Corporation, 3400 Outer Drive West, Detroit, MI 48239-4001
83. M. H. Haselkorn, Caterpillar Inc., Technical Center, Bldg.E, P.O. Box 1875, Peoria, IL 61629
84. G. S. Hausmann, UTRC, Silver Lane, East Hartford, CT 06108
85. N. A. Henein, Wayne State University, College of Engineering, Center for Automotive Research, Detroit, MI 48202
86. S. J. Hinkle, Detroit Diesel Corporation, 13400 Outer Drive West, Detroit, MI 48239-4001
87. J. W. Hodgson, Professor, Mechanical and Aerospace Engineering Dept., University of Tennessee, 414 Dougherty Hall, Knoxville, TN 37996-2210
88. Robert Ingel, Naval Research Laboratory, 4555 Overlook Avenue, S.W. Code: 63-70, Washington, D.C. 20375
89. M. J. Jennings, Ricardo-ITI, Inc., 645 Blackhawk Drive, Westmont, IL 60559
90. L. Johnson, Argonne National Laboratory, 9700 South Cass Avenue, 362-2B, Argonne, IL 60439
91. Roy Kamo, President, Adiabatics, Inc., 639 S. Mapleton, Columbus, IN 47201
92. Dr. Robert N. Katz, Army Materials and Mechanics Research Center, Arsenal Street, Watertown, MA 02172
93. P. M. Laing, Detroit Diesel Corporation, 134000 Outer Drive West, Detroit, MI 48239-4001
94. James Lankford, Southwest Research Institute, Department of Material Sciences, P.O. Drawer 28570, 6220 Culebra Drive, San Antonio, TX 78284
95. R. P. Larsen, Argonne National Laboratory, 9700 S. Cass Avenue, 362-2B, Argonne, IL 60439
96. H. J. Larson, Caterpillar Inc., Technical Center, Bldg. L, 100 N. E. Adams, Peoria, IL 61629
97. S. R. Levine, NASA Lewis Research Center, 21000 Brookpark Road, MS 49-3, Cleveland, OH 44135
98. James McCandless, Kohler Company, Kohler, WI 53044
99. Robert Miller, NASA Lewis Research Center, MS 49-3, Cleveland, OH 44135
100. S. P. Miller, Detroit Diesel Corporation, 13400 Outer Drive West, Detroit MI 48239-4001
101. Henry K. Ng, Cummins Engine Company, Mail Code 50180, Columbus, IN 47202-3005
102. R. C. Novak, UTRC, Silver Lane, East Hartford, CT 06108
103. James W. Patten, Cummins Engine Company, Mail Code 50183, Columbus, IN 47202-3005
104. Perkins Engines, Inc., Engineering Department, 24175 Research Drive, Farmington, MI 48024
105. Dr. Roy Rice, W.R. Grace and Company, 7379 Route 32, Columbia, MD 21044
106. R. B. Schulz, DOE, Office of Transportation Materials, Forrestal Bldg., CE-151, Washington, D.C. 20585
107. E. E. Schwarz, (AMSTA _RGR), U. S. Army TACOM, 11 Mile Road, Warren, MI 48397-5000

108. Gurpreet Singh, Internal Combustion and Gas Turbine Division, Code: 56X31, NAVSEA, Washington, D.C. 20362-5101
109. Dr. W. E. Snyder, Waukesha Engine Division, Dresser Industries, P.O. Box 379, Waukesha, WI 53167
110. J. D. Spuller, John Deere and Company, John Deere Road, Moline, IL 61265
111. T. Strom, NASA Lewis Research Center, MS 87-6, 21000 Brookpark Road, Cleveland, OH 44135
112. D. H. Reichenbach, Cummins Engine Company, Mail Code 50193, Columbus, IN 47202-3005
113. W. R. Wade, Ford Motor Company, P.O. Box 2053, Dearborn, MI 48121
114. Karen E. Weber, Detroit Diesel Corporation, 13400 Outer Drive West, Detroit, MI 48239
115. C. D. Weiss, Caterpillar Inc., Tech Center, Bldg. E, P.O. Box 1875, Peoria, IL 61656
116. D. G. Wirth, Coors Porcelain Company, Director, Technical Operations, Golden, CO 80401
117. V. W. Wong, Building 31, Rm. 155, Massachusetts Institute of Technology, Sloan Automotive Engine Laboratory, 77 Massachusetts Avenue, Cambridge, MA 02139
118. J. C. Wood, NASA Lewis Research Center, MS 86-6, 21000 Brookpark Road, Cleveland, OH 44135
119. T. M. Yonushonis, Cummins Engine Company, P.O. Box 3005, Mail Code 50183, Columbus, IN 47202-3005
120. Office of Assistant Manager for Energy Research and Development, DOE-Oak Ridge Operations, Oak Ridge, TN 37831

121-132. Technical Information Center, DOE, P.O. Box 62, Oak Ridge, TN 37831